

Article

Raman Spectroscopic Studies of Pyrite at High Pressure and High Temperature

Juan Chen ¹, Heping Li ^{2,*}, Yi Yuan ³, Mengxue Zhang ¹, Shuhang Shuai ¹ and Jingjing Wan ¹

¹ School of Chemical Engineering, Guizhou Institute of Technology, Guiyang 550003, China; chenjuan0445@git.edu.cn (J.C.); 2018070102@stu.git.edu.cn (M.Z.); 2018070123@stu.git.edu.cn (S.S.); 2019070117@stu.git.edu.cn (J.W.)

² Key Laboratory of High-Temperature and High-Pressure Study of the Earth's Interior, Institute of Geochemistry, Chinese Academy of Sciences, Guiyang 550081, China

³ Analysis and Testing Center, Guizhou Institute of Technology, Guiyang 550003, China; yuanyi@git.edu.cn

* Correspondence: liheping@vip.gyig.ac.cn

Abstract: Variations in the Raman spectra of pyrite were studied from 113 to 853 K at room pressure with a Linkam heating and freezing stage, and for 297–513 K and pressures up to 1.9 GPa with a hydrothermal diamond anvil cell. All observed frequencies decreased continuously with an increase in temperatures up to 653 K at ambient pressure. Hematite began to form at 653 K, all pyrite had transformed to hematite (H) at 688 K, and the hematite melted at 853 K. An increase in temperature at every initial pressure (group 1: 0.5 GPa, group 2: 1.1 GPa, group 3: 1.7 GPa, group 4: 1.9 GPa), showed no evidence for chemical reaction or pyrite decomposition. Two or three Raman modes were observed because of crystal orientation or temperature-induced fluorescence effects. The pressure groups showed a decreasing trend of frequency with gradual heating. The interaction of pressure and temperature led to a gradual decrease in Ag and Eg mode at a lower pressure (0.5 GPa and 1.1 GPa) than other pressure groups. Pressure and temperature effects are evident for groups 1 and 2; however, for groups 3 and 4, the temperature shows a larger effect than pressure and leads to a sharp decrease in Ag and Eg modes.

Keywords: pyrite; Raman spectroscopy; high pressure; high temperature



Citation: Chen, J.; Li, H.; Yuan, Y.; Zhang, M.; Shuai, S.; Wan, J. Raman Spectroscopic Studies of Pyrite at High Pressure and High Temperature. *Minerals* **2022**, *12*, 332. <https://doi.org/10.3390/min12030332>

Academic Editors: Lidong Dai, Haiying Hu, Jianjun Jiang and Jordi Ibanez-Insa

Received: 27 January 2022

Accepted: 3 March 2022

Published: 8 March 2022

Publisher's Note: MDPI stays neutral with regard to jurisdictional claims in published maps and institutional affiliations.



Copyright: © 2022 by the authors. Licensee MDPI, Basel, Switzerland. This article is an open access article distributed under the terms and conditions of the Creative Commons Attribution (CC BY) license (<https://creativecommons.org/licenses/by/4.0/>).

1. Introduction

The most common sulfide mineral pyrite FeS_2 , which is common in ore deposits and results in acid mine drainage because of its specific physical and chemical properties, has attracted the interest of many researchers in the high-pressure and high-temperature field.

As with NaCl, pyrite has a cubic structure, with a non-symmorphic space group $T_h^6(\text{Pa}3)$ and four formula units per unit cell. The Fe atoms and center of the S_2 pairs (in the dumb-bell structure) occupy face-centered cubic lattice sites [1,2]. According to group ($\text{Pa}3$) theory, the irreducible representation of FeS_2 vibrations is expressed as $\Gamma = \text{Ag} + \text{Eg} + 3\text{Tg} + 2\text{Au} + 6\text{Tu}$, and the $\text{Ag} + \text{Eg} + 3\text{Tg}$ represents five Raman active modes [1]. These expressions indicate that one mode is (Ag , S–S in phase stretch) symmetric and one is doubly degenerate (Eg , S_2 librational mode), and the third is triply degenerate (Tg , $\text{Tg}(1)$ and $\text{Tg}(3)$ are coupled librational and stretching modes with $\text{Tg}(2)$ being the S–S out-of-phase stretching mode). When the Raman signals of pyrite were excited by the 514.5-nm line of an argon-ion laser, the assignment of all Raman modes included Eg : 344 cm^{-1} , $\text{Tg}(1)$: 350 cm^{-1} , $\text{Tg}(2)$: 377 cm^{-1} , Ag : 379 cm^{-1} , and $\text{Tg}(3)$: 430 cm^{-1} , which is a typical structure of anisotropic pyrite, according to Kleppe and Jephcoat [2].

Ambient Raman research on pyrite has been undertaken since the 1970s [1,3–5]. It has been suggested that pyrite has type-I and type-II Raman frequency positions [5], and three or fewer modes have been observed [3–5], depending on the crystal orientation, sample purity, sample surface smoothness, and laser source. Vogt et al. [1] proposed the complete

first-order Raman spectra of pyrite, for the first time, by theoretical interpretation of the phonon frequencies.

Thermogravimetric analysis (TGA) and differential thermal analysis (DTA) have been used extensively to research the thermodynamic properties of pyrite at a high temperature and room pressure [6–12]. Schoenlaub [6] suggested the decomposition of pyrite by TGA and DTA in different gases. They found that pyrite decomposes to sulfur vapor and pyrrhotite in neutral (N_2) or reducing gas (e.g., CO). It transforms to sulfur dioxide and ferrous sulfide between 718 K (445 °C) and 793 K (520 °C), and then sulfur dioxide and hematite above 893 K (620 °C) in oxygen, and shows a less pronounced reaction activity in air but has a greater activity at higher temperatures. Pyrite reacts with carbon dioxide slowly and transforms to magnetite. According to Jorgensen and Moyle [7], a periodic thermal instability exists when pyrite particles are oxidized in air at 723 K (450 °C); the TGA and DTA results show that the sample temperature was unstable in the first 40 min and the XRD result demonstrated the presence of hematite and pyrite, with temperatures ranging between 643 K (370 °C) and 753 K (480 °C). Music et al. [8] studied the thermal decomposition of pyrite by XRD and ^{57}Fe Mossbauer spectroscopy in air and found that hematite, maghemite, and pyrrhotite were the thermal decomposition products of natural pyrite; only hematite was present above 673 K (400 °C). Fegley et al. [10] studied pyrite decomposition kinetics in pure CO_2 and impure CO_2 gas and found that pyrite transforms to pyrrhotite (Fe_7S_8) or more Fe-rich pyrrhotites, to magnetite (Fe_3O_4) by oxidation, to maghemite ($\gamma-Fe_2O_3$), and finally to hematite ($\alpha-Fe_2O_3$). Li and Zhang [13] proposed temperature dependence susceptibilities of pyrite in argon and air and found that pyrite transforms to magnetic minerals (magnetite and pyrrhotite) when heated to 653 K (380 °C).

High-pressure studies of pyrite are also interesting [2,14–17]. Pyrite is structurally stable to 55 GPa at static pressure and to 320 GPa in shock wave experiments. Cervantes et al. [15] found that the band gap of FeS_2 decreased linearly with pressure at -1.13×10^{-2} eV/GPa to 28 GPa. According to the linear trend, FeS_2 is expected to metallize at a pressure of 80 (± 8) GPa. Kleppe and Jephcoat [2] described the Raman shift variation in pyrite under hydrostatic and non-hydrostatic conditions to 55 GPa at room temperature. Liu et al. [17] conducted research on the electrical conductivity at high temperature and pressure. They found that the electrical conductivities of natural pyrite increased with pressure, and the increasing trend strengthened after ~ 13 GPa, which correlates to the energy level of the trace element Co in pyrite.

Simultaneous high-pressure and high-temperature studies of pyrite have been undertaken [16,17]. Liu et al. [17] described the variation in the electrical conductivity up to 573 K and from 1 atm to 20.9 GPa. They found that the electrical conductivity increased with temperature at a constant pressure, and so does the pressure, and no evidence of chemical reaction or structural phase transition of pyrite was detected by Raman spectroscopy. Yuan and Zheng [16] found that the positive dependence of A_g and E_g modes on pressure indicates a stress-induced contraction of S–S and Fe–S bonds, whereas the negative dependence on temperature shows their temperature-induced expansion. The thermal expansion coefficient was derived from the Raman spectra of pyrite up to 2.1 GPa and 675 K. A 20 wt.% NaCl solution was used as the pressure-transmitting medium by Yuan and Zheng [16].

A study of pyrite at 113–873 K and atmospheric pressure by Raman spectra has not been developed adequately. Therefore, this study aims to establish the Raman spectroscopic characteristics of FeS_2 pyrite under the abovementioned conditions. The Raman spectra of pyrite from 0.1 MPa to 2 GPa and up to 553 K under hydrostatic conditions is also inadequate, and further detailed study is necessary to confirm the dominating factor of pressure and/or temperature on Raman shifts.

2. Materials and Methods

Pyrite samples were collected from Longsheng Ethnic Minorities Autonomous County in Guangxi. The mineral phase of the pyrite was confirmed by an X'Pert Pro X-ray

diffractometer (Phillips Company, Amsterdam, The Netherlands), with a purity above 99.0%, and the chemical composition of major pyrite (Table 1) was determined by a EPMA-1600 electron probe microanalyzer (Shimadzu, Kyoto, Japan) in the State Key Laboratory of Ore Deposit Geochemistry, Institute of Geochemistry, Chinese Academy of Sciences. Some samples were cut to 10 mm × 10 mm × 0.2 mm and polished on both sides for high- and low-temperature experiments on a heating and freezing stage. Other samples were ground to pass through an 80 mesh sieve for simultaneous high-pressure and high-temperature experiments in a hydrothermal diamond anvil cell (HDAC).

Table 1. Chemical composition of major pyrite analyzed with EPMA (wt.%).

Pyrite	S (%)	Fe (%)	Hg (%)	Mo (%)	Au (%)	Co (%)	Pb (%)	Zn (%)	Total (%)
No.1	52.43	46.37	1.08	0.47	0.00	0.10	0.11	0.06	100.62
No.2	52.77	46.49	0.56	0.57	0.20	0.11	0.10	0.06	100.87
No.3	52.64	45.97	0.66	0.51	0.34	0.09	0.07	0.00	100.28
No.4	52.54	46.18	0.00	0.50	0.05	0.09	0.12	0.18	99.67
average	52.60	46.25	0.57	0.51	0.15	0.10	0.10	0.07	100.36

The spectra were excited by the 514.5 nm line of a Spectra-Physics 2017 laser (Newport Corporation, Irvine, CA, USA) and collected through a Renishaw InVia Raman spectrometer (Renishaw, London, England) in the Key Laboratory of High-Temperature and High-Pressure Study of the Earth's Interior, Institute of Geochemistry, Chinese Academy of Sciences, the spectrometer resolution was $\pm 1 \text{ cm}^{-1}$.

2.1. High- and Low-Temperature Experiments

The sample was placed directly on a quartz window in a Linkam THMSG600 heating and freezing stage (Linkam Scientific Instruments, Tadworth, UK). Liquid nitrogen purging was used to protect the stage and provide low temperatures of 113 K–273 K. A platinum resistor sensor was used as a heater to provide high temperatures at 273 K–873 K. The temperature was monitored by a platinum (10%) rhodium/platinum Type-S thermocouple that was attached to the heater. The temperature resolution was 0.01 K, and the temperature was stable to $\pm 0.1 \text{ K}$.

In the heating and cooling studies at room pressure, the working parameters of the Raman spectrometer included the exposure time of 10 s, a 2-times accumulations, laser power of 20 MW, spectrum range of 100–1500 cm^{-1} , and objective of SLM PLAN 20×.

2.2. Simultaneous High-Pressure and High-Temperature Experiments

Heating in the HDAC can be achieved with small resistance furnaces around the diamond anvils. The HDAC is similar to a Bassett-type [18] externally heated diamond anvil cell. A 0.3-mm-thick stainless-steel sheet (model T301) was used as a gasket and the sample chamber was 0.3–0.4 mm in diameter and placed between the two 0.8-mm culets as a sandwich. A methanol–ethanol ratio of 4:1 was loaded into the HDAC chamber with a single quartz crystal. The experimental pressure was calculated from Equation (1) according to the Raman shift of the 464 cm^{-1} peak of quartz [19], the uncertainty of the pressure was $\pm 50 \text{ MPa}$ at 23 °C. The difference in frequency of the 464 cm^{-1} line at the experimental temperature T and the frequency at 23 °C is described in the α -quartz stability field by Equation (2), where $-196 \leq T \text{ (}^\circ\text{C)} \leq 560$.

$$P(\text{MPa}) = 0.36079 \times [(\Delta\nu_P)_{464}]^2 + 110.86 \times (\Delta\nu_P)_{464} \quad (1)$$

$$(\Delta\nu_T)_{464, P=0.1\text{MPa}} (\text{cm}^{-1}) = 2.50136 \times 10^{-11} \times T^4 + 1.46454 \times 10^{-8} \times T^3 - 1.801 \times 10^{-5} \times T^2 - 0.01216 \times T + 0.29 \quad (2)$$

The sample was heated by small furnaces made of Ni₉₀Cr₁₀ alloy wires and the temperature was measured by a Ni₉₀Cr₁₀–Ni₉₅Si₅ thermocouple, which was calibrated

by referring to the melting points of $C_6H_5NH(COCH_3)$ (acetanilide, 388 K (115 °C)) and $C_{20}H_{14}O_4$ (phenolphthalein, 535.6 K (262.6 °C)) at atmospheric pressure before the experiment. The uncertainty of the temperature was ± 2.5 K in the range of 273 K–553 K (0–280 °C).

In the simultaneous high-pressure and high-temperature study, the following Raman spectrometer parameters were used: 30 s exposure time, 2-times accumulation, 80 MW laser power, 100–1000 cm^{-1} spectral range, and SLM PLAN 20 \times of objective.

3. Results and Discussion

3.1. High- and Low-Temperature Study of Pyrite at Ambient Pressure

The Raman peak assignment of pyrite is given in Table 2 [2]. Only three Raman active modes of pyrite were observed (Eg, Ag, Tg(3)), which agrees with most studies. Sometimes only two modes, Eg and Ag, were observed, which depended on crystal orientation perpendicular to the laser emission.

Table 2. Ambient Raman bands (cm^{-1}) of pyrite at 298 K.

ν_0 (cm^{-1}) (This Study)	ν_0 (cm^{-1}) (Kleppe and Jephcoat [2])	Comments	Symmetries and Assignments
342	344	Weak and need peak separation	Eg, S ₂ libration
348	350		Tg(1), coupled libration and stretch
378	379	377 cm^{-1} is covered by 379 cm^{-1}	Ag, S–S in phase stretching Tg(2), S–S out-of-phase stretching
429	430	Appear in certain orientations and lower temperature	Tg(3), coupled libration and stretch

A weakened Raman peak signal that was caused by the fluorescence effects of high temperature was observed, but limited effects resulted for the low-temperature condition, which is supported by the low-temperature study of pyrite. The Raman frequencies for the Eg, Ag, and Tg(3) bands of pyrite decreased with an increase in temperature in Figures 1 and 2, which is consistent with the results of Yuan and Zheng [16].

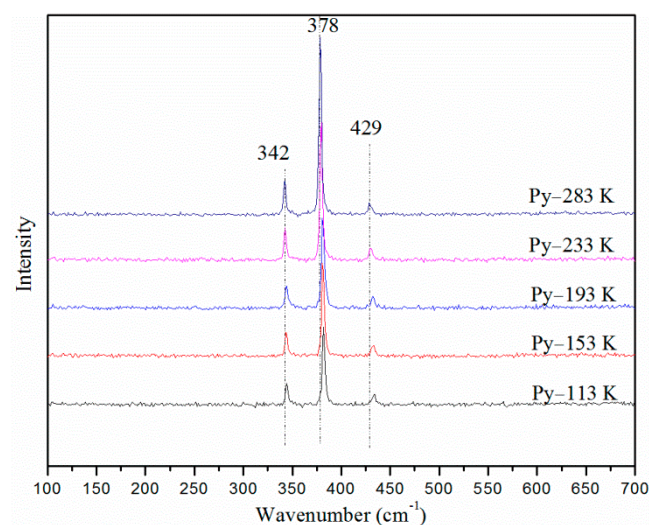


Figure 1. Raman shift of pyrite during cooling (113–283 K).

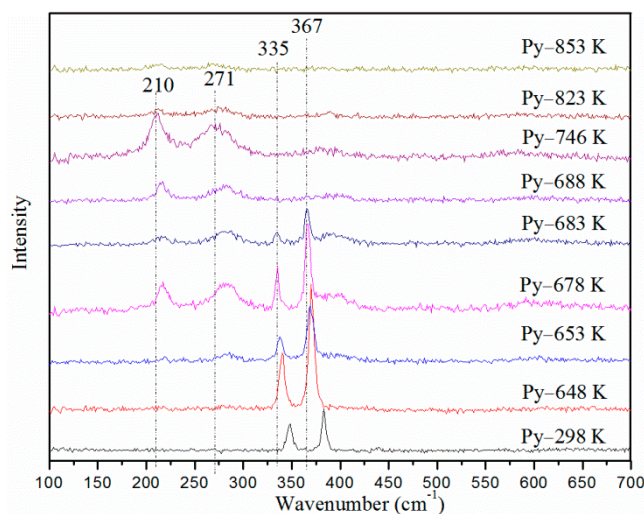


Figure 2. Raman shift of pyrite during heating (298–853 K).

The Eg, Ag, and Tg(3) Raman wavenumbers are shown in Figure 3. The quadratic temperature dependence is within the experimental error. The parameters that were derived by quadratic and linear regressions of all modes are shown in Tables 3 and 4. The temperature dependence of the Ag mode is larger than that in Eg mode ($-0.0366 \text{ cm}^{-1}/\text{K}$ compared with $-0.0245 \text{ cm}^{-1}/\text{K}$), which led to obvious separation between them with temperature, because the Ag (in the phase S–S stretching frequency) mode was determined mainly by the S–S force constant [20] and the Eg (librational frequency) was largely governed by the Fe–S force constant. Temperature induces faster molecule vibrations and a decreasing S–S and Fe–S bond energy. The Tg(3) mode disappeared above 303 K because of the weakened Raman signal at the high temperature (Figure 3). It was not known whether a chemical reaction or phase transition resulted because no new frequencies appeared. At 653 K, two new peaks were observed: (H-(Eg(2) + Eg(3))) represents the mixture modes of Eg(2) and Eg(3) of hematite, and H-A1g(1) represents the A1g(1) mode of hematite. At 688 K, the Ag and Eg modes of pyrite disappeared, which left two new peaks until 853 K. It is speculated that the new frequencies represent hematite from the Raman library [21]. To confirm the new phase, we conducted another experiment, where the temperature was reduced gradually to 293 K after it had been increased to 703 K. Figure 4 compares the pyrite product to a previous study on hematite [22], and the two spectra appeared consistent, except for the broader peak and high background in this study.

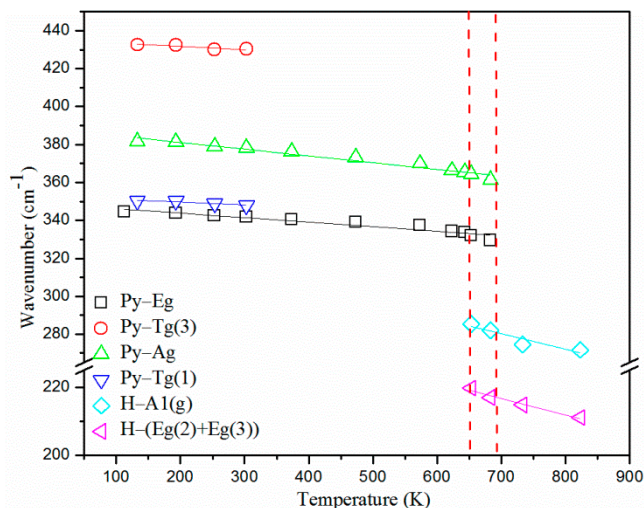


Figure 3. Wavenumber of six peak variations with increasing temperature.

Table 3. Variable modes of Raman bands ($\Delta\nu$) of pyrite with increasing temperature according to $\nu_i = aT^2 + bT + c$. ν_i and $\Delta\nu$ are in cm^{-1} , T in K, a and b have the corresponding units, c is a constant, and R^2 is the correlation coefficient.

ν_i (cm^{-1})	$\Delta\nu$	$a \times 10^5$	$b \times 10^2$	c	R^2
Eg: 329.94	−14.432	−4	1.09	342.91	0.9780
Tg(1): 347.87	−2.393	−9	2.72	347.97	0.8504
Ag: 361.25	−20.302	−5	0.78	381.01	0.9907
Tg(3): 430.28	−2.405	7	−4.66	437.99	0.8599
H-(Eg(2) + Eg(3)): 274.19	−11.201	−4	1.09	342.91	0.9780
H-A1g(1): 211.04	−8.675	20	−32.84	353.89	0.9709

Table 4. Variable modes of Raman bands ($\Delta\nu$) of pyrite with increasing temperature according to $\nu_i = aT + c$. ν_i and $\Delta\nu$ are in cm^{-1} , T in K, a in cm^{-1}/K , c is a constant, and R^2 is the correlation coefficient.

ν_i (cm^{-1})	$\Delta\nu$	a (cm^{-1}/K)	c	R^2
Eg: 329.94	−14.432	−0.0245	348.49	0.9394
Tg(1): 347.87	−2.393	−0.0129	352.05	0.7549
Ag: 361.25	−20.301	−0.0366	388.13	0.9654
Tg(3): 430.28	−2.405	−0.0181	435.09	0.8289
H-(Eg(2) + Eg(3)): 274.19	−11.201	−0.0788	336.08	0.8123
H-A1g(1): 211.04	−8.675	−0.0505	251.91	0.9426

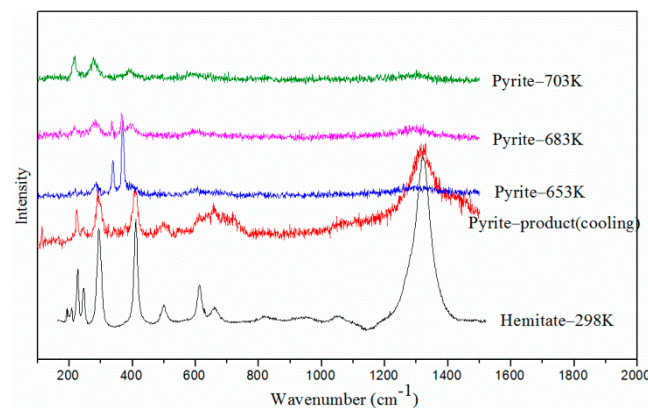


Figure 4. Raman spectra of pyrite and hematite from bottom to top: hematite at 298 K [22], increased pyrite temperature to 703 K and cooling to 298 K, pyrite at 683 K, pyrite at 703 K.

Pyrite began to transform to hematite from oxidation at 653 K. At ambient conditions, the hematite phonon frequencies were A1g(1): 224 cm^{-1} , Eg(1): 243 cm^{-1} , Eg(2): 290 cm^{-1} , Eg(3): 297 cm^{-1} , Eg(4): 408 cm^{-1} , A1g(2): 496 cm^{-1} , and Eg(5): 609 cm^{-1} (Shim and Duffy, 2001). Two broad and strong peaks were visible: 285 cm^{-1} represents a mixture of Eg(2) and Eg(3), and 219 cm^{-1} represents A1g(1) in the high-temperature study. Figure 2 shows the phase transformation from pyrite to hematite according to the Raman shift. Pyrite and hematite coexist at 653 K. At 688 K, the Eg and Ag modes of pyrite disappeared. The poor crystal of hematite resulted in melting at 823 K and the hematite melted at 853 K, where no signal was observed because of the temperature-induced fluorescence effect and weak focus of melts.

The high-temperature Raman study of pyrite by Linkam heating and cooling indicates that pyrite decomposed to hematite between 653 K and 688 K. The results from this study are distinct from a previous study [6] but like those of Jorgensen and Moyle [7], and Music et al. [8] as shown in Figure 5. Jorgensen and Moyle [7] reported the presence of hematite between 643 K ($370 \text{ }^\circ\text{C}$) and 753 K ($480 \text{ }^\circ\text{C}$); Similarly, hematite was present at

673 K (400 °C) according to Music et al. [8]. The difference in temperatures for hematite’s presence between this study and the two abovementioned experiments could have resulted from an inconsistent heating rate. This study may provide more accurate data by virtue of the advanced Linkam heating and freezing stage technology. Further studies will be required to check the effect of heating rate on the decomposition temperature.

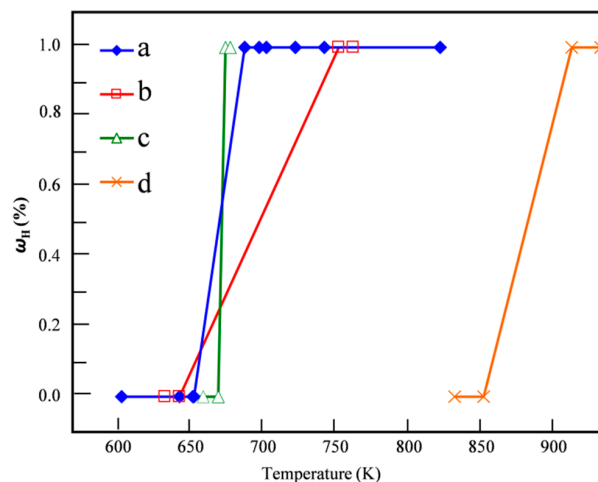


Figure 5. Hematite content produced as a product of pyrite with increasing temperature, ω_H represents the mass fraction of hematite. (a) Present work (solid diamond). (b) Jorgensen and Moyle [7] (open square). (c) Music et al. [8] (open triangle). (d) Schoenlaub [6] (red cross).

The full width at half maximum (FWHM) of six bands displays the temperature dependence (Figure 6). The FWHM of all pyrite modes broadens with an increase in temperature, but the hematite modes (H-A1g(1) and H-(Eg(2) + Eg(3))) increase sharply with an increase in temperature because the hematite that is produced by pyrite at a high temperature has a poor crystal structure and rough surface.

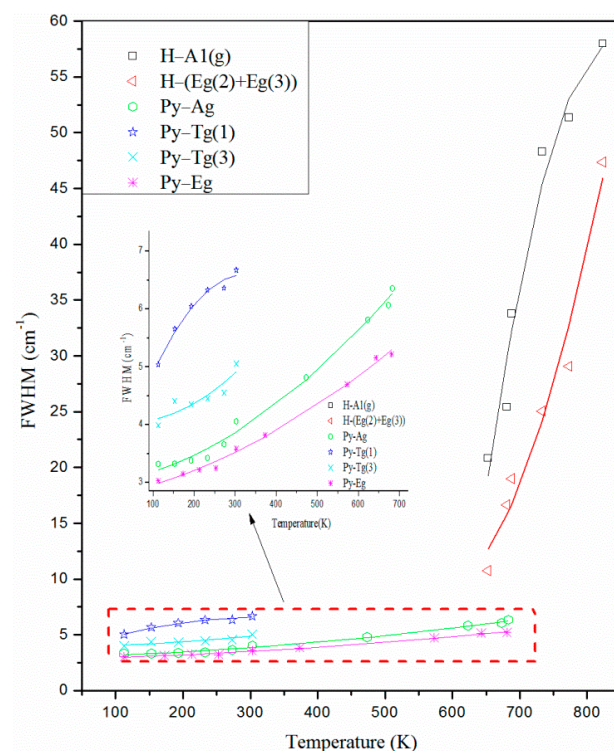


Figure 6. FWHM of six bands’ variation with increasing temperature.

3.2. Simultaneous High-Temperature and High-Pressure Study of Pyrite

Water reacts with pyrite as a function of temperature, pressure, and time. To avoid the reaction between water and pyrite, methanol–ethanol (4:1) was used as a pressure medium instead of a 20 wt.% NaCl solution [16] to provide hydrostatic pressure. The synthetic quartz Raman band [19] was measured as a pressure calibrant in this study. High-temperature experiments were conducted at four different initial pressures (group 1: 0.5 GPa, group 2: 1.1 GPa, group 3: 1.7 GPa, group 4: 1.9 GPa). A common feature was observed in Figure 7, i.e., pressure increases slowly to 453 K. The cell's mechanical properties were influenced above 453 K and resulted in an induced decrease in pressure. Test replication would help to improve the data, so that pressure variation that is associated with this condition is negligible.

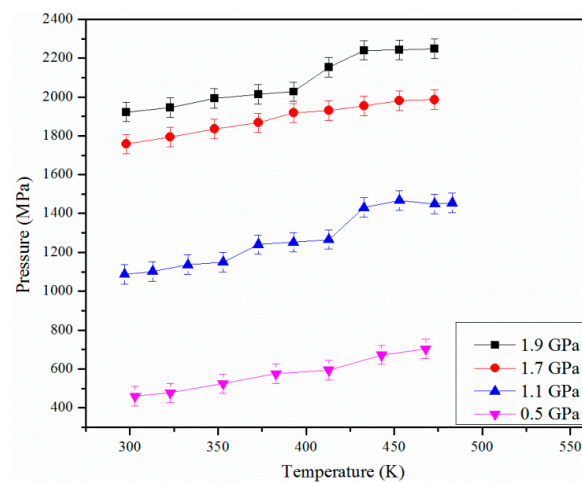


Figure 7. Various initial pressures, pyrite heating in HDAC from 298 K–493 K, in situ pressures (0.5, 1.1, 1.7, 1.9 GPa) at every temperature point. Error bars show pressure uncertainty is ± 50 MPa.

Both the temperature and pressure effect have an impact (Figure 8), and the Ag and Eg mode shifts to being faster for groups 4 and 3 than for groups 1 and 2. The positive pressure and negative temperature dependence of the two modes suggests that the pressure and temperature effects are identically strong at a lower pressure (see groups 1 and 2), and the temperature dependence is more obvious at a higher pressure (see groups 3 and 4).

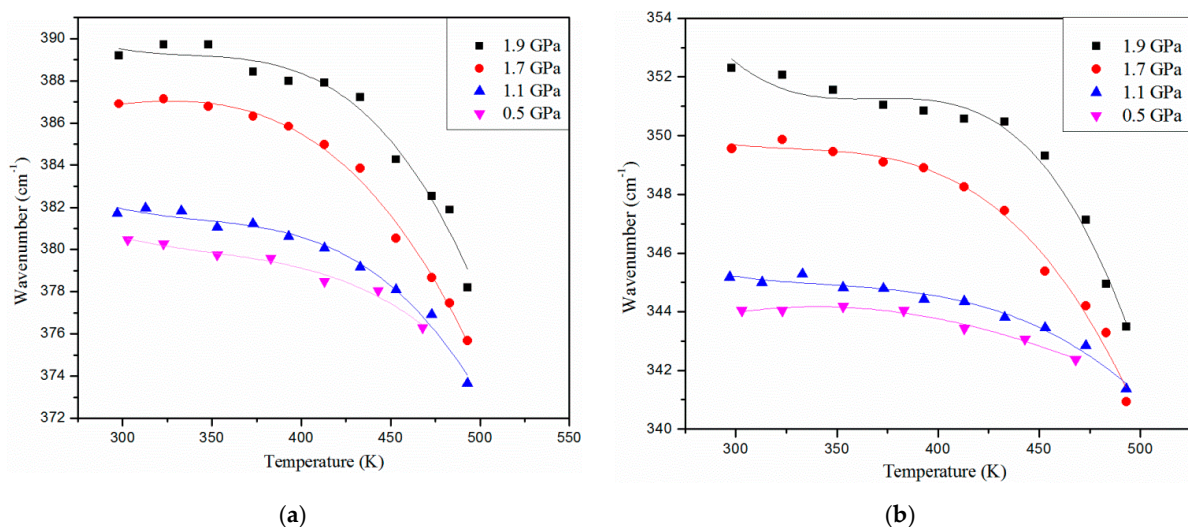


Figure 8. (a) Raman shift of A(g) mode heating at different initial pressures: 0.5, 1.1, 1.7, 1.9 GPa; (b) Raman shift of E(g) mode heating at different initial pressures: 0.5, 1.1, 1.7, 1.9 GPa.

4. Conclusions

All observed pyrite frequencies decreased continuously with an increase in temperature to 653 K at room pressure. Pyrite transformed to hematite at 653 K, had fully changed to hematite at 688 K, and the hematite melted at 853 K. At the four initial pressures (0.5, 1.1, 1.7, 1.9 GPa) and with an increasing temperature, there was no evidence for chemical reaction or decomposition. Every group demonstrated a frequency decline with gradual heating. The interaction of pressure and temperature led to a gentle decrease in Ag and Eg modes at a lower pressure (0.5 and 1.1 GPa) than other groups. The positive pressure and negative temperature dependence of the two modes suggests that the pressure and temperature effect are identically strong at a lower pressure (0.5 and 1.1 GPa), and the temperature dependence is more prominent at a higher pressure (1.7 and 1.9 GPa).

Author Contributions: Methodology, J.C. and H.L.; software, Y.Y.; resources and data curation, M.Z., S.S. and J.W.; writing—original draft preparation, J.C.; writing—review and editing, H.L.; funding acquisition, J.C. and H.L. All authors have read and agreed to the published version of the manuscript.

Funding: This research is supported by the fund from the Science and Technology Agency of Guizhou province, China ([2020]1Y170 and [2019]2830).

Data Availability Statement: Not applicable.

Acknowledgments: The authors thank Terry Mernagh for grammar modification.

Conflicts of Interest: The authors declare no conflict of interest.

References

1. Vogt, H.; Chattopadhyay, T.; Stolz, H.J. Complete first-order Raman spectra of the pyrite structure compounds FeS₂, MnS₂ and SiP₂. *J. Phys. Chem. Solids* **1983**, *44*, 869–873. [\[CrossRef\]](#)
2. Kleppe, A.K.; Jephcoat, A.P. High-pressure Raman spectroscopic studies of FeS₂ pyrite. *Mineral. Mag.* **2004**, *68*, 433–441. [\[CrossRef\]](#)
3. Ushioda, S. Raman scattering from phonons in iron pyrite (FeS₂). *Solid State Commun.* **1972**, *10*, 307–310. [\[CrossRef\]](#)
4. Anastassakis, E.; Perry, C.H. Light scattering and IR measurements in XS₂ pyrite-type compounds. *J. Chem. Phys.* **1976**, *64*, 3604–3609. [\[CrossRef\]](#)
5. Mernagh, T.P.; Trudu, A.G. A laser Raman microprobe study of some geologically important sulphide minerals. *Chem. Geol.* **1993**, *103*, 113–127. [\[CrossRef\]](#)
6. Schoenlaub, R.A. Oxidation of pyrite. *J. Am. Ceram. Soc.* **1969**, *52*, 40–43. [\[CrossRef\]](#)
7. Jorgensen, F.; Moyle, F.J. Periodic thermal instability during the isothermal oxidation of pyrite. *Metall. Mater. Trans. B* **1981**, *12*, 769–770. [\[CrossRef\]](#)
8. Music, S.; Popović, S.; Ristić, M. Thermal decomposition of pyrite. *J. Radioanal. Nucl. Chem.* **1992**, *162*, 217–226. [\[CrossRef\]](#)
9. Inge, I.M.; Jan, Y.; Heidi, V.; Dirk, V.F.; Jules, M.; Lucien, C.V.P.; Grazyna, G.; Piotr, W. Study of coal-derived pyrite and its conversion products using atmospheric pressure temperature-programmed reduction (AP-TP). *Energy Fuels* **1995**, *9*, 950–955.
10. Fegley, B., Jr.; Lodders, K.; Treiman, A.H.; Klingelhöfer, G. The rate of pyrite decomposition on the surface of Venus. *Icarus* **1995**, *115*, 159–180. [\[CrossRef\]](#)
11. Corradi, A.B.; Leonelli, C.; Manfredini, T.; Romagnoli, M. Quantitative determination of pyrite in, ceramic clay raw materials by DTA. *Thermochim. Acta* **1996**, *287*, 101–109. [\[CrossRef\]](#)
12. Yi, P.; Yu, Q.; Zong, H. Thermodynamic analysis for chemical desulfurization of pyrite in coal. *Coal Convers.* **1999**, *22*, 47–52.
13. Li, H.; Zhang, S. Detection of mineralogical changes in pyrite using measurements of temperature-dependence susceptibilities. *Chin. J. Geophys.* **2005**, *48*, 1384–1391. [\[CrossRef\]](#)
14. Merkel, S.; Jephcoat, A.P.; Shu, J.; Mao, H.; Gillet, P.; Hemley, R.J. Equation of state, elasticity, and shear strength of pyrite under high pressure. *Phys. Chem. Miner.* **2002**, *29*, 1–9. [\[CrossRef\]](#)
15. Cervantes, P.; Slanic, Z.; Bridges, F.; Knittle, E.; Williams, Q. The band gap and electrical resistivity of FeS₂-pyrite at high pressures. *J. Phys. Chem. Solids* **2002**, *63*, 1927–1933. [\[CrossRef\]](#)
16. Yuan, X.; Zheng, H. In situ Raman spectroscopic studies of FeS₂ pyrite up to 675 K and 2100 MPa using a hydrothermal diamond anvil cell. *Mineral. Mag.* **2015**, *79*, 1–10. [\[CrossRef\]](#)
17. Liu, K.; Dai, L.; Li, H.; Hu, H.; Wu, L.; Zhuang, Y.; Pu, C.; Yang, L. Migration of impurity level reflected in the electrical conductivity variation for natural pyrite at high temperature and high pressure. *Phys. Chem. Miner.* **2018**, *45*, 85–92. [\[CrossRef\]](#)
18. Bassett, W.A. High pressure-temperature aqueous systems in the hydrothermal diamond anvil cell (HDAC). *Eur. J. Mineral.* **2003**, *15*, 773–780. [\[CrossRef\]](#)
19. Schmidt, C.; Ziemann, M.A. In-situ Raman spectroscopy of quartz: A pressure sensor for hydrothermal diamond-anvil cell experiments at elevated temperatures. *Am. Mineral.* **2000**, *85*, 1725–1734. [\[CrossRef\]](#)

20. Lutz, H.D.; Zwinscher, J. Lattice dynamics of pyrite FeS_2 -polarizable-ion model. *Phys. Chem. Miner.* **1996**, *23*, 497–502. [CrossRef]
21. Database of Raman Spectra. X-ray Diffraction and Chemistry Data for Minerals. Available online: <https://rruff.info/hematite/display=default/R050300> (accessed on 10 January 2022).
22. Shim, S.; Duffy, T. Raman spectroscopy of Fe_2O_3 to 62 GPa. *Am. Mineral.* **2002**, *87*, 318–326. [CrossRef]